Polymer Chemistry

Accepted Manuscript

ROYAL SOCIETY OF CHEMISTRY

www.rsc.org/polymers

Cite this: DOI: 10.1039/c0xx00000x

www.rsc.org/xxxxxx

PAPER

Thermo-responsive Gold/poly(vinyl alcohol)-*b*-poly(*N*-vinylcaprolactam) Core/corona Nanoparticles as Drug Delivery System †

Ji Liu,[a,c] Christophe Detrembleur,*[a] Marie Hurtgen,[a] Antoine Debuigne,[a] Marie-Claire De Pauw-Gillet,[b] Stéphane Mornet,[c] Etienne Duguet *[c] and Christine Jérôme*[a]

Received (in XXX, XXX) Xth XXXXXXXXX 20XX, Accepted Xth XXXXXXXXX 20XX
DOI: 10.1039/b000000x

Core-corona gold/poly(vinyl alcohol)-*b*-poly(*N*-vinylcaprolactam) nanoparticles (gold@PVOH-*b*-PNVCL NPs) were fabricated via an *in-situ* method, where a gold salt was reduced within the macromolecular aqueous solution. Arrangement of macromolecular chains on the surface of gold cores was studied by transmission electron microscopy (TEM), X-ray photoelectron spectroscopy and infrared spectroscopy. Responsiveness to temperature and preserved colloidal stability of the gold@PVOH-*b*-PNVCL NPs above the lower critical solution temperature (LCST) were confirmed by dynamic light scattering and turbidity measurement. The drug loading capacity (*DLC* of *ca*. 1.3-2.8 *wt*. %) of the gold@PVOH-*b*-PNVCL NPs as a drug delivery system (DDS) was tested with Nadolol®, a hydrophilic drug, and the release behaviours were studied under several temperatures. PVOH-*b*-PNVCL copolymers with LCST of few degrees above biological temperature (37 °C), for example, $PVOH_{180}$-*b*-$PNVCL_{110}$ (LCST of 41 °C), are preferential, due to the relative slower release at 37 °C, but faster release under temperatures of few degrees higher. Cytocompatibility of the gold@PVOH-*b*-PNVCL NPs against mouse fibroblastic L929 cells was evaluated via the MTS assay. Cellular uptake within MEL-5 human melanoma cells was studied by confocal laser scanning microscope, fluorescence-activated cell sorting and TEM techniques; and it showed that gold@PVOH-*b*-PNVCL NPs preferably accumulated within the cellular cytoplasm, with an incubation concentration and period-dependent uptake process. All these results corroborated a general utility of these thermo-responsive gold@PVOH-*b*-PNVCL NPs for drug delivery and controlled drug release.

Introduction

Nano-scaled particles have been widely proposed as potential drug delivery systems (DDS), due to their distinguished capability to accumulate within the tumor sites via enhanced permeation and retention effect (EPR).[1, 2] Within those DDS, chemotherapeutics are usually loaded by encapsulation or attachment via covalent bonding, coordination, electrostatic interaction or van der Waals interaction, *etc*. An ideal DDS is expected to stably trap the cargoes, *i.e.* non-leaking, during the period of both storage and circulation within the biological fluids. However, it is supposed to become labile once targeting to the desirable sites, followed with a controlled drug release.[3] Typically, compared with the normal tissues, some pathological microenvironments manifest themselves with distinctive characters, such as difference in temperature or pH, presence of some biomolecules, *etc.*, leading to the use of these pathological characters as stimuli to trigger the drug release. In the last decade, different kinds of nano-scaled vehicles have been reported as potential DDS, such as polymer micelles,[4-7] organic/inorganic hybrid nanoparticles,[8-17] mesoporous silica nanoparticles,[18] to cite only a few. Among them, stimuli-responsive organic/inorganic nanoparticles are gaining increasingly more investigation due to their as-expected combination of intrinsic properties from both inorganic core and stimuli-responsive organic corona. On the other side, those stimuli-responsive components are known to be capable of changing their physico-chemical properties in response to those as-mentioned pathological stimuli, accompanying with the release of those pre-loaded cargoes. Therefore, stimuli-triggered release, specially in those pathological microenvironments, is accomplished.[3]

Gold nanoparticles (GNPs) have been extensively and intensively investigated in the biomedical field thanks to their low toxicity essence, outstanding chemical stability, versatile surface functionality, size- and shape-dependent optical features, *etc*.[19, 20] However, it is of great importance to modify their surface in order to improve their colloidal and serum stability before the clinical practices. Up to now, some stimuli-responsive macromolecules have been attempted to stabilize the GNPs via physical or chemical routes and find their applications in phototherapy, photoacoustic imaging agents, light-activated drug release,[8, 12, 14, 15, 20, 21] to cite a few. Among them, *N*-vinylcaprolactam (NVCL)-based and *N*-isopropylacrylamide (NIPAM)-based macromolecules have attracted much attention recently due to their distinctive thermo-responsive properties.[22-29] In most cases, these thermo-responsive macromolecules display a

lower critical solution temperature (LCST) in aqueous solution. Namely, below the LCST, water is a good solvent for these macromolecular chains, which are hydrated with a randomly-coiled conformation; while above the LCST, water becomes a poor solvent, thus the macromolecular chains are dehydrated and adopt a globular conformation.[3] As reported,[30] temperature of the tumour microenvironments is always 2-3 °C higher than that of the surrounding normal tissue by virtue of the faster blood circulation, particularly in the peripheral region. Therefore, the thermo-responsive components impart those polymer-coated GNPs with promising potential as smart DDS for temperature-triggered release, especially for tumour treatment. On the other hand, considering the nano-scaled dimension of these polymer-coated GNPs, a higher accumulation could also be achieved, leading to an improved targeting effect and higher therapeutic efficiency.

In-situ preparation of nanoparticles is a versatile and effective method to fabricate inorganic nanoparticles in the presence of stabilizers. With selected molecules *in-situ* bonding to the surface of inorganic nanoparticles, new hybrid nanoparticles can be easily obtained.[21, 31, 32] Additionally, decorating inorganic nanoparticles with biocompatible macromolecules might make the as-formed integrity more suitable for biomedical application. Herein, well-defined thermo-responsive poly(vinyl alcohol)-*b*-poly(*N*-vinylcaprolactam) copolymers (PVOH-*b*-PNVCL), prepared via the cobalt-mediated radical polymerization (CMRP) strategy,[33-35] were used as stabilizer, and gold@PVOH-*b*-PNVCL NPs were prepared via the *in-situ* method (Scheme 1). Optical properties of the gold@PVOH-*b*-PNVCL NPs were investigated with UV/*vis* spectroscopy under different temperatures, while thermo-responsive properties by DLS and turbidity measurements. Nadolol®, a hydrophilic and non-selective beta blocker for the treatment of high blood pressure, migraine headaches and chest pain,[36] was loaded into the polymer corona, and the release behaviours under different temperatures were studied. Cytotoxicity of the gold@PVOH-*b*-PNVCL NPs against the fibroblast L929 cell line was evaluated via the MTS assay; while preliminary studies on cellular uptake into MEL-5 human melanoma cells were performed with confocal laser scanning microscope (CLSM), fluorescence-activated cell sorting (FACS) and TEM techniques.

Experimental Details

Preparation of those macromolecules

PVOH-*b*-PNVCL block copolymers were obtained by hydrolysis of poly(vinyl acetate)-*b*-poly(*N*-vinylcaprolactam) copolymers, which were synthesized via CMRP technique according to a previously reported procedure.[33] $PVOH_{226}$-*b*-$PNVCL_{494}$ (Polym#1) and $PVOH_{180}$-*b*-$PNVCL_{110}$ (Polym#2) were selected for the following studies. The detailed physicochemical features of the PVOH-*b*-PNVCL copolymers used in this work are summarized in Table 1. FITC-labelled PVOH-*b*-PNVCL copolymer (FITC: fluorescein isothiocyanate isomer I) was prepared from the reaction between PVOH-*b*-PNVCL copolymer and FITC (VOH/FITC = 100/3 *mol*.) in anhydrous DMSO under N_2 atmosphere for 12 h. The as-prepared copolymer was purified by precipitating into cold diethyl ether and dried under vacuum at room temperature. $PVOH_{168}$ homopolymer (M_w/M_n = 1.09) was obtained via the CMRP technique described previously,[37] while $PNVCL_{213}$ homopolymer (M_w/M_n = 2.40, Polym#3) was synthesized via conventional free-radical polymerization of NVCL monomer with AIBN initiator at 60 °C in anhydrous DMF.

In-situ preparation of gold@PVOH-*b*-PNVCL NPs

Typically, 0.5 mL of $HAuCl_4 \cdot 3H_2O$ aqueous solution (10 mM) and 2 mL of PVOH-*b*-PNVCL solution (0.2 *wt*. %) were added sequentially into a round flask under stirring (200 rpm) at room temperature, prior to the injection of 50 μL of fresh $NaBH_4$ solution (100 mM). The color of the mixture turned into dark red immediately, indicating the formation of gold nanoparticles. The resultant gold@PVOH-*b*-PNVCL NPs were purified by three centrifugation-rinsing cycles (10,000 rpm, 10 min), and then re-dispersed in PBS buffer solution (10 mM, pH 7.4) under sonication (5 min). Gold@PNVCL, gold@PVOH and FITC-labelled gold@PVOH-*b*-PNVCL NPs were also prepared via the same protocol.

Drug loading and release behaviours

Nadolol®-loaded gold@PVOH-*b*-PNVCL NPs were prepared by dispersing gold@PVOH-*b*-PNVCL NPs in Nadolol® aqueous solution and stirring overnight. After two centrifugation/rinsing cycles (6000 rpm, 10 min), the purified Nadolol®-loaded gold@PVOH-*b*-PNVCL NPs were re-dispersed in PBS buffer solution (10 mM, pH 7.4); while the centrifugation supernatants were collected, and drug loading amount was estimated by measuring the UV/*vis* absorbance at 270 nm. A calibration curve was established by plotting the absorbance of standard solutions *vs*. concentration from 0 to 300 mg L^{-1} (see ESI, Fig. S1†). Drug loading capacity (*DLC*) was used to evaluate the drug loading performance of the gold@PVOH-*b*-PNVCL NPs as DDS:

$$DLC\% = \frac{mass\ of\ loaded\ Nadolol^{@}}{mass\ of\ gold@PVOH\text{-}b\text{-}PNVCL\ NPs}$$

Release profiles of the Nadolol®-loaded gold@PVOH-*b*-PNVCL NPs were followed via the traditional dialysis strategy. 5 mL of Nadolol®-loaded gold@PVOH-*b*-PNVCL NPs suspension (2 mg mL^{-1}) was sealed in a dialysis membrane (cut-off: 3,500 g mol^{-1}), and then dialyzed against 10 mL of PBS buffer solution (10 mM, pH 7.4) under gentle stirring at different temperatures. At each pre-determined interval, 0.2 mL of the release medium was sampled for UV/*vis* measurement, while 0.2 mL of fresh medium was fed to keep a constant volume. All those release profiles were presented in a cumulative mode, and the bar graphs in each figure were presented as mean value ± standard deviation from three independent experiments.

Cell culture and cytotoxicity assessment

The mouse fibroblast L929 cell line was obtained from ATCC (*ATCC* CCL-1) and grown at 37 °C under humidified air containing 5 *vol*. % of CO_2 in GIBCO Dulbecco's modified eagle medium (DMEM, 4.5 g L^{-1} of glucose), which was supplemented with 5 *vol*. % of fetal bovine serum (FBS, Gibco), 1 *vol*. % of GlutaMax, 1 *vol*. % of penicillin/streptomycin (10,000 units of penicillin (base) and 10,000 units of streptomycin (base) mL^{-1}) (DMEM complete medium). The human melanoma MEL-5 cell line (originated from a non pigmented clone 32, gift from Dr. G.

Degiovanni, University of Liège) was cultured in DMEM complete medium and detached with trypsin (0.2 *vol*. %)/PBS buffer solution (Ca^{2+}/Mg^{2+} free).

Cytotoxicity assessment was carried out following the well-established MTS assay. L929 cells were seeded in 96-well plates with a density of 5×10^3 cells $well^{-1}$ and grown in DMEM complete medium for another 24 h. Then the cells were treated with gold@PVOH-*b*-PNVCL NPs suspensions with different concentrations (200, 100, 10 and 1 μg mL^{-1}) for 24 and 48 h. For each condition, 5 parallel duplicates were repeated at the same time. After a pre-determined incubation period, the cells were rinsed with PBS buffer solution (Ca^{2+}/Mg^{2+} free) and cell viability was assessed following the MTS assay. Specifically, 20 μL of MTS in 100 μL of PBS buffer solution (with Ca^{2+}/Mg^{2+}) were added, and then the cells were incubated for 30 min at 37 °C. The absorbance of each well at 490 nm was measured using a Power wave X (Biotek instrument *Inc*.) micro-plate reader. Percentages of cell viability were determined relative to the untreated cells (control, 100% viability).

Cellular uptake into MEL-5 melanoma cells

Qualitative studies on cellular uptake via confocal laser scanning microscope (CLSM, Nikon, A1R hybrid resonant) was carried out with MEL-5 cells internalized with FITC-labelled gold@PVOH-*b*-PNVCL NPs. MEL-5 cells (3.8×10^5) were seeded in a 12-well plate with 1.5 mL of DMEM complete medium. After 24-h incubation, the medium was replaced with 1.5 mL of fresh DMEM complete medium (untreated) or FITC-labelled gold@PVOH-*b*-PNVCL NPs suspension (50 μg mL^{-1}) in DMEM complete medium (treated). After incubating for a pre-determined period, the medium was removed and the cells were rinsed twice with PBS buffer (Ca^{2+}/Mg^{2+} free) to eliminate those free nanoparticles. Then the cells were treated with paraformaldehyde (4 *vol*. %)/DAPI (1 *vol*. %)/PBS buffer solution (Ca^{2+}/Mg^{2+} free) at room temperature for another 15 min in dark. Finally, after rinsing twice with PBS buffer solution (Ca^{2+}/Mg^{2+} free), 1 mL of fresh PBS buffer solution (with Ca^{2+}/Mg^{2+}) was added. Analysis of the treated MEL-5 cells was conducted with a Nikon CLSM (*Ex*: 488 nm, *Em*: 525 nm).

Qualitative studies on cellular uptake via TEM (Philips CM-100 microscope) were also carried out with the treated MEL-5 cells, which were obtained according to the above-mentioned protocol. After the treated cells were detached with trypsin (0.2 *wt*. %)/PBS buffer solution (Ca^{2+}/Mg^{2+} free), centrifuged (1300 rpm, 5 min) and re-dispersed in fresh PBS buffer solution (Ca^{2+}/Mg^{2+} free), the cell pellet was fixed with glutaraldehyde (4 *wt*. %)/PBS buffer solution (Ca^{2+}/Mg^{2+} free). After 24 h, the pellet was rinsed with PBS buffer solution (Ca^{2+}/Mg^{2+} free) again in order to remove the free fixatives, and then dehydrated in an alcohol series, embedded in Epon, and sliced for TEM observation.

Quantitative studies on cellular uptake via cytofluorometer (FACS canto II, BD biosciences) measurement were also performed with the treated MEL-5 cells, which were also obtained according to the above-mentioned protocol. After detachment with trypsin (0.2 *vol*. %)/PBS (Ca^{2+}/Mg^{2+} free) buffer solution and centrifugation (1300 rpm, 5 min), the treated cells were re-dispersed in 400 μL of fresh PBS buffer solution (with Ca^{2+}/Mg^{2+}). The analysis was conducted with a fluorescence-activated cell sorter (FACS, Becton-Dickinson), while untreated MEL-5 cells were taken as a blank. The fluorescence intensities and the percentage of cell-associated fluorescence were determined by using the CellQuest software. The ratio of fluorescence intensity per 10,000 treated MEL-5 cells to that of 10,000 untreated cells was expressed as mean fluorescence intensity (MFI), and then used to evaluate the cellular uptake efficiency.

Statistical analysis

The cell culture experiments were performed in triplicate. Results are presented as mean value ± standard deviation. Statistical analysis of the data was performed using the Student's *t*-test, and statistical significance was determined at $p < 0.05$.

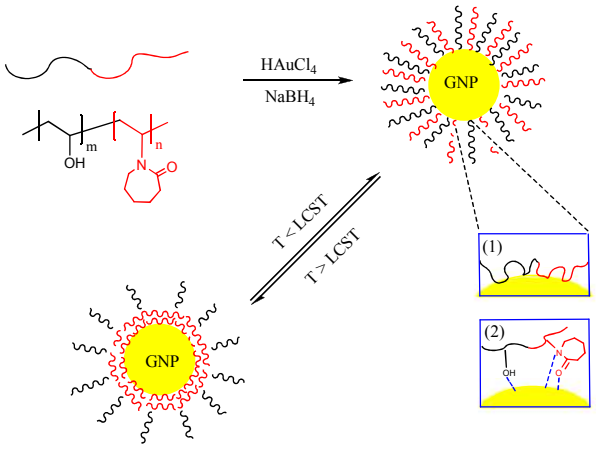

Scheme. 1 Schematic illustration of *in-situ* synthesis of gold@PVOH-*b*-PNVCL NPs and different conformations of both PVOH (black) and PNVCL (red) segments (tail, loop and train, (1)) on the GNP surface, interaction between the gold and oxygen or nitrogen atoms (2), as well as the corresponding phase and conformational change when exposed to variation in temperature.

Results and discussion

Preparation of gold@PVOH-*b*-PNVCL NPs

PVOH-*b*-PNVCL copolymers were synthesized via the cobalt-mediated radical polymerization (CMRP) technique,[34, 35] according to our previous report.[33] Here, two PVOH-*b*-PNVCL copolymers with different compositions and LCST values were used to synthesize gold@PVOH-*b*-PNVCL NPs (samples S#1 and S#2, Table 1), as well as PNVCL homopolymer for gold@PNVCL NPs (sample S#3, Table 1). To establish the specific interaction between tetrachloroauric anions ($AuCl^{4-}$) and PVOH-*b*-PNVCL copolymers, UV/*vis* spectrum of a mixture solution, comprising of $HAuCl_4$ (0.5 mL, 10 mM) and PVOH-*b*-PNVCL (2 mL, 0.2 *wt*. %), was recorded and compared with that of pure $AuCl^{4-}$ ion aqueous solution. The interaction was evidenced by the red shift of the intrinsic absorption band of Au ions (see ESI, Fig. S2a†). This is in agreement with the previous reports,[38-40] which claimed that gold atoms can be easily chelated by nitrogen and oxygen atoms. However, no nanoparticles were detected by TEM in this mixture after 1-h mixing, indicating the incapability of the PVOH-*b*-PNVCL copolymer to spontaneously reduce the $AuCl_4^-$ ions. After addition of $NaBH_4$, the solution turned dark immediately and later red, corresponding to the nucleation and growth of gold nanoparticles, respectively. The *in-*

situ growth of gold NPs was monitored by UV/*vis* spectroscopy

Table 1 Parameters for gold@PVOH-*b*-PNVCL NPs and the corresponding PVOH-*b*-PNVCL copolymers with different compositions

Samples	gold@PVOH-*b*-PNVCL					PVOH-*b*-PNVCL used		
	D_h [a] nm	*PDI* [a]	D_{TEM} nm	Polymer content [b] *wt*. %	*DLC* [c] %	Structure	M_w/M_n [d]	LCST °C
S#1	100	0.22	25	17.1	2.8	$PVOH_{226}$-*b*-$PNVCL_{494}$	1.06	37
S#2	110	0.24	23	14.1	1.3	$PVOH_{180}$-*b*-$PNVCL_{110}$	1.10	41
S#3	130	0.31	25	16.6	-	$PNVCL_{213}$	2.40	34

[a] mean hydrodynamic diameter and size distribution of the polymer coated gold NPs was determined at 25 °C by dynamic light scattering (DLS)
[b] the polymer content was confirmed by TGA
[c] drug loading capacity was estimated from the formula given in the experimental part
[d] molecular weight polydispersity was determined by SEC in DMF of the PVAc-*b*-PNVCL precursors

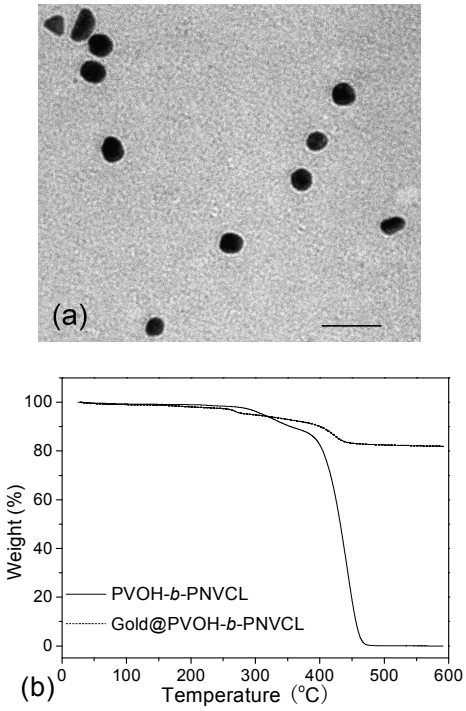

Fig. 1 Representative TEM image of gold@PVOH-*b*-PNVCL NPs (S#1) (scale bar: 50 nm) after negative staining (a); TGA traces of S#1 and corresponding $PVOH_{226}$-*b*-$PNVCL_{494}$ pure copolymer (Polym#1) under air (b).

during the whole reaction period (see ESI, Fig. S2b†). Upon reduction, a single surface plasmon resonance (SPR) band arose at *ca*. 530 nm, which is the characteristic SPR band for gold nanospheres.[19] Later, red-shift and broadening of the SPR band were detected, due to the increase in nanoparticles size and formation of irregular morphologies, as shown in the TEM picture of S#1 (Fig. 1a). A final average size of *ca*. 25 nm was statically estimated. The appearance of irregular morphologies might also suggest the incapability of the PVOH-*b*-PNVCL copolymers in controlling the shape of gold cores. In addition, polymer corona can be clearly observed after negative staining. D_h of *ca*. 100 nm (PDI 0.22) was measured by DLS (see ESI, Fig. S3a†) for S#1, which is much larger than that from TEM, since the hydrated and swelling polymer corona converted into a dense and collapsed polymer shell after drying. Presence of gold core and polymer corona was proved by XRD (see ESI, Fig. S3b†) and XPS (see ESI, Fig. S3c and S3d†) analysis, respectively, and the polymer content was confirmed to be *ca*. 17 *wt*. % by TGA for S#1 (Fig. 1b). Additionally, parameters for other gold NPs (S#2 and S#3) were all listed in Table 1.

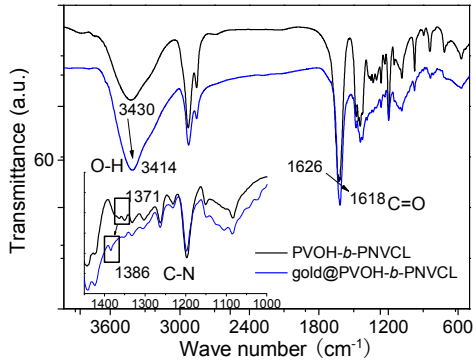

Fig. 2 FTIR spectra of pure $PVOH_{226}$-*b*-$PNVCL_{494}$ copolymer (Polym#1) and gold@PVOH-*b*-PNVCL NPs (S#1), inset: partially-magnified FTIR spectra in the range of 1000-1500 cm^{-1}, as well as signal assignment of those transmission peaks of interest.

The comparison of FTIR spectra of both S#1 and the corresponding $PVOH_{226}$-*b*-$PNVCL_{494}$ pure copolymer shows remarkable shifts upon coating the PVOH-*b*-PNVCL copolymer onto the gold cores (Fig. 2): the peak at 1628 cm^{-1}, which is ascribed to the typical C=O (ν_s) band of the cyclic amide in PNVCL block, shifted to 1615 cm^{-1}; the peak corresponding to pendant hydroxyl groups (ν_s) in PVOH block at 3440 cm^{-1} shifted to 3420 cm^{-1}; and C-N bond in PNVCL block shifted from 1371 cm^{-1} to 1386 cm^{-1}. This observation indicates that electron densities of the C=O, O-H and C-N bond are affected by the presence of gold cores. Thus, interaction between gold and both PVOH and PNVCL blocks was confirmed and the conformation of loop, train and tail of these two blocks on the gold surface were proposed as shown in Scheme 1. Basing on our speculations that part of the polymer chains interact with the gold cores, theoretically, a doubling of each band should be observed: one for the interacting bonds and one for the non-interacting ones. Here, we tried to amplify the FTIR signals to see whether there is some doubling of the signals of interest; however only a shift of the overall peak is observed. This phenomenon could probably be attributed to overlay of the two peaks, the resolution limitation of FTIR technique and limited polymer fraction in the samples, *etc*.

The finding from FTIR analysis here is in sharp contrast to those sulfur-ended macromolecules, which could easily be immobilized onto the gold surface by their chain-ends via Au-S conjugation, while the main macromolecular chains remain in the corona.[22-28] When we compared the FTIR spectra of $PVOH_{226}$-*b*-

$PNVCL_{494}$ pure polymer and $HAuCl_4/PVOH_{226}$-*b*-$PNVCL_{494}$ mixture, signal-shifting was also detected in Fig. S4†. Similar phenomena were also reported for gold@polymer nanoparticles with different polymer coatings, such as gold@polyaniline NPs,[41] and gold@poly(benzyl ether) dendrons NPs,[42] *etc*. On the other side, we also made comparison of N1s and O1s signals from both pure PVOH-*b*-PNVCL (Polym#1) and gold@PVOH-*b*-PNVCL, as shown in Fig. S3e† and Fig. S3f†, respectively. Signal-shifting of 1.0, 0.3 and 0.9 eV was observed for N1s and O1s (C-O) and O1s (C=O) signal, respectively. Similar XPS signal-shifting phenomena were also reported on poly (vinyl pyrrolidone) (PVP) or PNVCL-coated gold nanocrystals,[43] PVP-coated silver nanowires,[44] PVP-coated platinum nanoparticles,[45] due to the interaction between metallic atoms and nitrogen and/or oxygen atoms. Therefore, these data support that the PVOH-*b*-PNVCL macromolecular chains immobilize onto the surface of the gold cores through the interaction between gold atoms and O or N atoms, as already reported.[38-40] Moreover, this interaction could also account for the SPR band shifting in the UV/*vis* spectrum of $HAuCl_4/PVOH_{226}$-*b*-$PNVCL_{494}$ mixture (see ESI, Fig. S2a†).

Thermo-responsiveness of gold@PVOH-*b*-PNVCL NPs

It is well-known that thermo-responsive polymers, such as those based on PNIPAAm or PNVCL, exhibit a rapid hydrated/dehydrated phase transition responding to temperature variation around the LCST, due to their hydrophobic essence above the LCST while hydrophilic below LCST.[3] In the case of gold@PVOH-*b*-PNVCL NPs, the dehydration of PVOH-*b*-PNVCL polymer chains should result in a denser polymer coating with decreased thickness. To investigate the thermo-responsiveness of the gold@PVOH-*b*-PNVCL NPs, effect of temperature on D_h and size polydispersity (PDI) was studied by DLS. Fig. 3a shows the dependence of D_h on temperature for gold@PVOH-*b*-PNVCL NPs (S#1) and gold@PNVCL NPs (S#3). For S#1, D_h slightly decreased and leveled off beyond 42 °C. Whereas for sample S#3, D_h exhibited a minimum at *ca*. 34 °C, and then increased continuously beyond its LCST, suggesting the aggregation of gold@PNVCL NPs due to their hydrophobic coating above the LCST. Additionally, taking the size distribution into consideration, a slight change was detected for S#1 above LCST (PDI of 0.22 at 25°C, 0.24 at 50 °C), while a sharp increase for S#3 due to the nanoparticles aggregation (PDI of 0.31 at 25 °C, 0.47 at 50 °C), similar to the gold@PNVCL[23] and gold@PNIPAAm[24] systems reported before. Thus, a superior stability against aggregation above LCST was confirmed for the gold@PVOH-*b*-PNVCL NPs.

Compared with those GNP@PNVCL[23] and GNP@PNIPAAm[24] systems reported previously, as well as the gold@PNVCL NPs we prepared here, difference in the stability above LCST of gold@PVOH-*b*-PNVCL NPs might arise from the stabilizing role of PVOH segments. As corroborated by FTIR analysis, both PVOH and PNVCL blocks interact with the gold core. Usually, at the interface, loop, train and tail conformation may be adopted for both PVOH and PNVCL segments due to the long chain length and high polymer concentration, as schematically illustrated in Scheme 1. When the temperature increased and exceeded LCST, PNVCL segments in all conformations might collapse due to their hydrophobic essence. Whereas, PVOH blocks might ideally adopt the same conformation, at the same time, they still serve as stabilizer via steric repulsion, despite of the collapsing of hydrophobic PNVCL segments (see ESI, Fig. S5a†). For gold@PNVCL NPs above LCST, the hydrophobic surface leads to the particle aggregation. While for S#1, steric repulsion from PVOH blocks contributes to a superior colloidal stability above LCST.

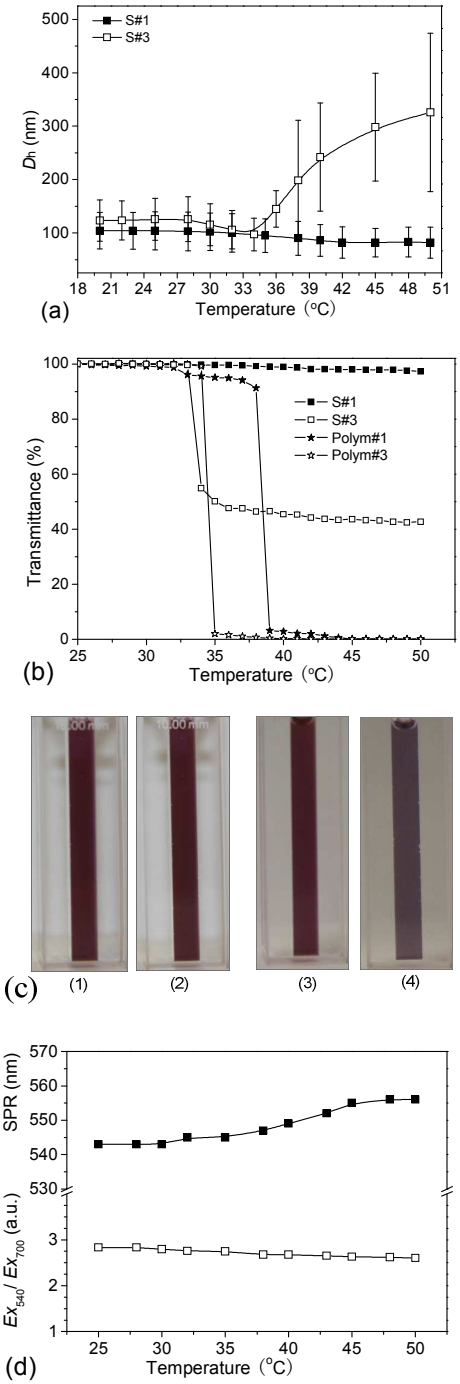

Fig. 3 Dependence of hydrodynamic diameters (D_h) for gold@PVOH-*b*-PNVCL (S#1, solid) and gold@PNVCL (S#3, open) on temperature (a); dependence of transmittance on temperature for S#1 and the corresponding $PVOH_{226}$-*b*-$PNVCL_{494}$ copolymer (Polym#1, 50 μg mL^{-1}) (b), pictures of gold@PVOH-*b*-PNVCL NPs suspension (S#1, 50 μg mL^{-1}) at 25 °C (c-1) and 50 °C (c-2), gold@PNVCL suspension (S#3) at 25 °C (c-3) and 50 °C (c-4); evolution of SPR band (solid) and extinction

ratio (Ex_{540}/Ex_{700}) (open) upon increasing temperature from 25 to 50 °C for S#1 (d). The solid lines just serve as eye guidance.

The ability of PVOH segments to stabilize the gold NPs was also evidenced by turbidity measurements as shown in Fig. 3b. The suspension of S#1 was transparent over the whole temperature range, while gold@PNVCL became turbid upon heating to 50 °C (Fig. 3c). Moreover, LCST detected by the turbidity measurement was slightly lower (*ca*. 1 °C) for gold@PNVCL NPs, compared with that of pure PNVCL homopolymer. This difference could be attributed to the reduced conformational freedom of PNVCL chains when immobilized on the surface of gold NPs, in agreement with some previous reports.[46, 47] Continuous heating/cooling treatment (see SEI, Fig. S5b†) also evidences good reversibility for the thermo-induced phase-transition of gold@PVOH-*b*-PNVCL NPs in aqueous suspension.

The UV/*vis* spectra were recorded for the suspension of S#1 from 25 to 50 °C as shown in Fig. S6a†. The change in SPR band was summarized in Fig. 3d, and the SPR wavelength remained stable below 37 °C (LCST 38 °C) while a red-shift was observed beyond. This kind of SPR red-shift for thermo-responsive gold nanoparticles have been reported previously;[24, 48-50] and the red-shift here could also be ascribed to the increase in the local refractive index and Rayleigh scattering coefficient, resulting from the collapsing of PNVCL segments. To evaluate the degree of aggregation, we used the extinction ratio (Ex_{540}/Ex_{700}) to study the stability of the gold@PVOH-*b*-PNVCL at different temperatures. As reported, this ratio was also a measure of colour for gold nanoparticles, with higher ratio for red while lower ratio for blue.[51] The change in Ex_{700}/Ex_{540} was summarized in Fig. 3d, and a slight change in the extinction ratio and nearly no obvious change in color (Fig. 3c-1 and 3c-2) were observed, due to the stable dispersion of S#1. On the contrary, for S#3 without PVOH block, a sharp increase in SPR band and extinction ratio (see SEI, Fig. S6b†), as well as color change from red (Fig. 3c-3) to purple (Fig. 3c-4) was detected, due to the particle aggregation.

Additionally, as reported, when gold NPs were brought into close contact with each other, the SPR band became broader due to the plasmon resonance coupling effect.[49, 50, 52] In the case of gold@PVOH-*b*-PNVCL (S#1), nearly no SPR band broadening is detected (see SEI, Fig. S6a†), compared to the gold@PNVCL (S#3, see SEI, Fig. S6b†) and gold@PNIPAAm NPs in those previous reports.[49, 50, 53] This may also indicate the absence of aggregation above LCST, in agreement with the results from both DLS and turbidity measurement. Furthermore, not only the change in transmittance (see SEI, Fig. S5b†), but also the temperature-induced red-shift (see SEI, Fig. S6c†) was reversible. Given the thermo-induced SPR red-shift and good reversibility under temperature flocculation, as well as superior stability above LCST for the gold@PNVCL-*b*-PVOH, we might conjecture this kind of gold nanoparticles might also be used as a biosensor, to detect the local temperature (above the LCST) with the plasmonic performance. Admittedly, it is only anticipation, and more investigation is still needed to support this potential use.

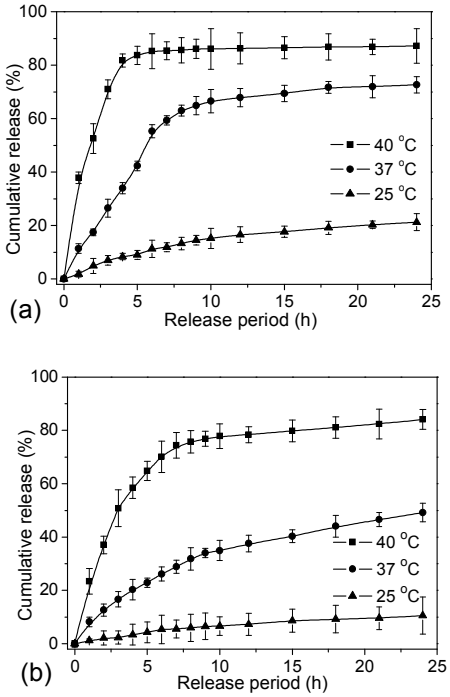

Fig. 4 Cumulative release profiles at different temperatures for Nadolol®-loaded gold@PVOH-*b*-PNVCL NPs, S#1 (a) and S#2 (b), the solid lines just serve as eye guidance.

Drug loading and release behaviours of gold@PVOH-*b*-PNVCL NPs

In order to evaluate the suitability of the gold@PVOH-*b*-PNVCL NPs as DDS for temperature-triggered release, Nadolol®, a hydrophilic drug which is expected to interact with the copolymer chains via H-bonding, was first loaded in the PVOH-*b*-PNVCL polymer corona of the nanoparticles. Then, the release behaviour under different temperature conditions was studied. Presence of Nadolol® in the drug-loaded gold@PVOH-*b*-PNVCL NPs was confirmed by UV/*vis* absorption spectroscopy (see SEI, Fig. S7†), and the amount of Nadolol® was estimated according to the calibration curve (see SEI, Fig. S1†). Since the polymer coating guides the drug loading capacity as well as the release behaviour, it is possible to tailor the loading and release performance by changing the composition of PVOH-*b*-PNVCL copolymers used. As expected, the drug loading capacity (*DLC*) for S#1 ($PVOH_{226}$-*b*-$PNVCL_{494}$, Polym#1) was confirmed to be *ca*. 2.8 *wt*. %, higher than that for S#2 ($PVOH_{180}$-*b*-$PNVCL_{110}$, Polym#2) of *ca*. 1.3 *wt*. %. Since the polymer fraction in the gold@PVOH-*b*-PNVCL NPs was similar for sample S#1 and S#2, we might ascribe the higher loading capacity of S#2 to the higher chemical composition of PNVCL segments. With the presence of carboxyl (C=O) groups in PNVCL segments, they are expected to show higher affinity to the Nadolol® molecules (-OH group), compared with hydroxyl groups (O-H) in PVOH. The relatively low loading capacity may be attributed to the weak Van der Waals interaction between the Nadolol® molecules and PVOH-*b*-PNVCL polymer corona, in line with *DLC* value reported on our previous DDS based on gold nanorod core with poly(ethylene glycol)-*b*-poly(*N*-vinylcaprolactam) corona.[28] It is deserved to note that, the primary goal of this current study is not to improve the drug loading capacity; but rather to develop a

novel temperature-triggered release system of the loaded cargoes, based on easily-derivatized copolymers bearing highly-hydrophilic PVOH and thermo-responsive PNVCL blocks. Emphasis will also be laid on the effect of chemical composition, as well as LCST of the PVOH-*b*-PNVCL copolymers, on the corresponding release behaviour, which will be investigated below.

Drug release profiles of S#1 under different temperatures (25, 37 and 40 °C) were followed in PBS buffer (10 mM, pH 7.4) and summarized in Fig. 4a. At 25 °C (below the LCST), *ca*. 20% of the loaded drug released within 24 h, in agreement with the diffusion-controlled mechanism. While for temperatures near or above the LCST, a faster release was detected. Similar release behaviours were also reported in other thermo-responsive DDS,[54, 55] due to the thermo-induced collapse of polymer corona and sneezing out of the cargo molecules. While incomplete release might be attributed to the trapping of drugs within the hydrophobic domain (see SEI, Fig. S8a†). Since the local temperature of tumour sites is *ca*. 2~3 °C higher than that of the surrounding tissue,[30] PVOH-*b*-PNVCL copolymers, with LCST matching the tumour site temperature, might exhibit a much more interesting release behavior. Here, gold NPs (S#2) coated with $PVOH_{180}$-*b*-$PNVCL_{110}$ (Polym#2, LCST of 41 °C) were also studied. As shown in Fig. 4b, a relative slower release was detected at 37 °C compared with that of S#1, suggesting lower leakage during the delivery; however, a faster release was observed at 40 °C. Thus, it might be conjectured that an optimal control over the chemical composition of polymer coating can improve the control over the drug release behaviours. In addition, drug release behaviour under a stepwise heating/cooling (40/37 °C) treatment was also studied in PBS buffer (pH 7.4, 10 mM) for drug-loaded gold@PVOH-*b*-PNVCL suspension from sample S#2 (see SEI, Fig. S8b†). Under alternating heating/cooling treatment, the PNVCL blocks may transit between the dehydrated and hydrated states. As expected, a faster release was observed at 40 °C while sustainable release at 37 °C, and nearly complete release after few-cycle temperature fluctuation between 37 and 40 °C, thanks to the alternating swelling/collapsing of the polymer corona. These results suggest the applicability of the gold@PVOH-*b*-PNVCL NPs as DDS of tumor chemotherapeutics, and the capability to address the complexity of biological systems with such temperature-regulated functionality. Additionally, as reported, gold nanoparticles could strongly absorb light with wavelength near the SPR band, and further convert the absorbed light to heat in a picosecond time scale. For those reasons, gold NPs have been considered to be promising for use in photothermal therapy as well as imaging in the biomedical field. Moreover, the local heating generated under laser irradiation has also been ingeniously utilized to trigger the drug release, to cite only a few. Therefore, the synergistic phototherapy and laser-induced chemotherapy could contribute a remarkable therapeutic efficiency. Considering the thermo-responsiveness of the polymer corona and as-confirmed thermo-induced drug release, the release of Nadolol® molecules from the gold@PVOH-*b*-PNVCL might also be activated under laser irradiation.

Cytotoxicity and cellular uptake of gold@PVOH-*b*-PNVCL NPs

Since the gold@PVOH-*b*-PNVCL NPs were targeting for *in vivo* DDS, it is of great significance for the DDS to possess good biocompatibility. Herein, cytotoxicity of the gold@PVOH-*b*-PNVCL NPs against fibroblasts L929 cell line was assessed via the MTS assay. In our previous test over reversibly cross-linked nanogels based on PVOH-*b*-PNVCL copolymers, no obvious cytotoxicity had been observed due to the good biocompatible essence of the two blocks.[5, 56] Herein, Fig. 5a and 5b showed that the cells viabilities were also not significantly affected after 24-h incubation, while slightly decreased after 48 h. Meanwhile, the cell viability was also demonstrated to be concentration-dependent; a slight decrease in cell viability was detected when the concentration was increased in the range of 1-200 μg mL^{-1}. The lower toxicity of the gold@PVOH-*b*-PNVCL NPs might also indirectly suggested that the PVOH-*b*-PNVCL polymer corona is not obviously desorbed during the cell culture; or comparable decrease in cell viabilities would be detected, as previously reported.[57]

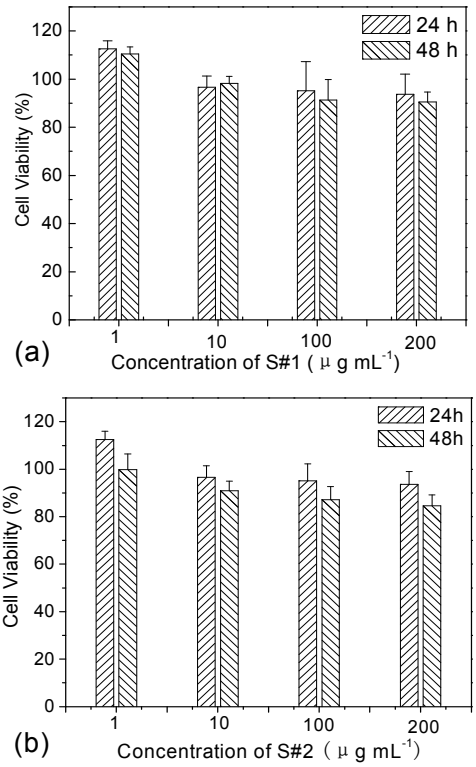

Fig. 5 Cell viabilities of fibroblasts L929 cell line against gold@PVOH-*b*-PNVCL NPs under different incubation concentrations and periods for S#1 (a) and S#2 (b), respectively; percentage cell viabilities of the L929 cells were expressed relatively to the untreated cells (control, 100%), and results were all presented as mean value ± standard deviation (n = 5).

To demonstrate the application of the gold@PVOH-*b*-PNVCL NPs as an efficient DDS, preliminary cell uptake studies were performed with human melanoma MEL-5 cell line, as a representative target for the DDS. Fluorescein isothiocyanate isomer I (FITC) was used as a convenient probe, owing to its accessible excitation and emission wavelengths and high reactivity with hydroxyl- or amine-bearing molecules. For the PVOH-*b*-PNVCL copolymer, FITC moieties were grafted to the

PVOH segments in anhydrous DMSO, and the grafting degree of 2.7 *mol.* % (proportion of PVOH-FITC units to the overall PVOH units) was confirmed by ^{1}H NMR analysis. Presence of fluorescent groups in the FITC-labelled gold@PVOH-*b*-PNVCL NPs were also confirmed by UV/*vis* absorption spectroscopy (see SEI, Fig. S7†). Cellular uptake and also distribution of FITC-labelled gold@PVOH-*b*-PNVCL NPs (50 mg L^{-1}) in MEL-5 cells were visualized with confocal laser scanning microscope (CLSM). Fig. 6a showed the CLSM image of MEL-5 cells after the nuclei were stained with DAPI (blue, Fig. 6a-1). Cellular uptake of the gold@PVOH-*b*-PNVCL NPs was confirmed by the presence of green luminescence in Fig. 6a-2. It is deserved to note that in the immerged image (Fig. 6a-4), most of the green luminescence was observed outside the nuclei, indicating the accumulation of gold@PVOH-*b*-PNVCL NPs within the cytoplasm, even though some of them localized close to the nuclear membrane. In addition, due to the incapacity for CLSM to distinguish nanoparticles internalized within the MEL-5 cells from those absorbed on the surface, TEM technique was further used to analyze the treated MEL-5 cells. As shown in Fig. 6b, nanoparticles, nearly the same size with the pristine gold@PVOH-*b*-PNVCL NPs (Fig. 1a), could be clearly observed inside an endosomal membrane in the cytoplasm, confirming the internalization of gold@PVOH-*b*-PNVCL NPs via endocytosis process.

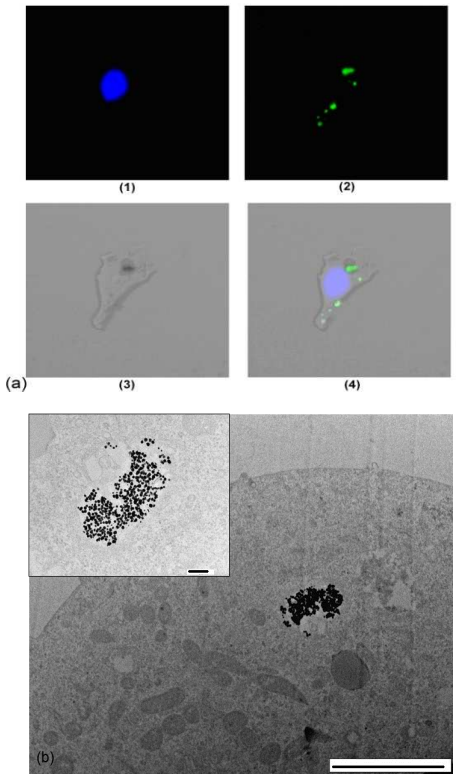

Fig. 6 Confocal laser scanning microscopic (CLSM) images of S#1-internalized MEL-5 cells after incubation with the FITC-labeled gold@PVOH-*b*-PNVCL NPs (50 μg mL^{-1}) for 6 h, cell nuclei stained with DAPI (blue, a-1), FITC-labeled gold NPs (green, a-2), phase contrast pattern (a-3), and the merged image (a-4); TEM image of the treated MEL-5 cells after 6-h incubation with gold@PVOH-*b*-PNVCL NPs (50 μg mL^{-1}, scale bar: 2000 nm), and inset: partially-magnified TEM image (scale bar: 200 nm) (b).

The gold@PVOH-*b*-PNVCL NPs internalized within MEL-5 cell were further analyzed via cytofluorometric measurement for a further understanding of the internalization kinetics. As shown in Fig. S9a†, after 6-h incubation, a big shift of the peak could also be detected in the FACS histogram, compared with the non-treated MEL-5 cells; and *ca*. 100% of the treated cells were internalized with gold@PVOH-*b*-PNVCL NPs. To quantify the cellular uptake of the gold@PVOH-*b*-PNVCL NPs, mean fluorescence intensity (MFI), denoted as the ratio of fluorescence intensity of 10,000 treated cells to that of 10,000 untreated cells, was used to study the concentration- and period-dependent uptake behaviours. As summarized in Fig. S9b†, a positive effect was observed for the dependence of MFI on both incubation period and incubation concentration, similarly to our previous finding on the internalization behaviours of γ-Fe_2O_3@poly(acrylic acid)-*b*-PVOH NPs[58] and GNR@poly(ε-caprolactone)-*b*-poly(ethylene glycol) NPs.[28] Thus, the uptake amount could be optimized via the control over the gold@PVOH-*b*-PNVCL NPs feeding amount and incubation period.

PVOH-coated gold NPs here, as well as those previously-reported PVOH-coated superparamagnetic nanoparticles (SPIONS),[57-61] exhibit a comparable biocompatibility to the commonly-used poly(ethylene glycol) (PEG) segments, indicating a great potential of PVOH as an idealistic biocompatible component. In addition to the biocompatibility, the *in vivo* circulation life of a DDS, *e.g.* liposome or nanoparticles, in the systemic circulation has been shown to highly depend on the surface hydrophobicity of the DDS, since hydrophobic nanoparticles are rapidly cleared by circulating monocytes, resulting in predominant localization in the livers.[62] Moreover, the nanoparticle surface, in contact with biological fluids, cells or cellular components, could be optimized to provide favourite or inert interactions with the cells. Coating nanoparticles with appropriate bioadhesion-resistant polymers, such as PEG and PVOH, *etc*., could greatly improve the ability to escape immune clearance process.[63] The role of PEG on the *in vivo* fate of PEGylated NPs has been well-established, like improving the colloidal and serum stability of the nanoparticles, increasing the attachment of dysopsonin proteins which suppress the phagocytic uptake, offering a non-specific surface for opsonin proteins binding in order to avoid uptake by reticulum-endothelial system (RES), *etc*.[63] Therefore, this kind of nanoparticles could remain stable with a longer *in vivo* circulating life, leading to a higher delivery efficiency.[63, 64] Even through the role and mechanism of PVOH has not been clearly revealed, there are still some reports dealing on the effect of PVOH corona on colloidal stability, uptaking efficiency and/or protein adsorption of the as-formed nanoparticles. Kimura and coworkers found that, the PVOH-coated liposomes (M_W: 20 000 g mol^{-1}) showed a comparable blood circulation time to those coated with PEG (M_W: 2000 g mol^{-1}).[65] Moreover, when PVOH was used to stabilized SPIONS, similar behaviors were also reported by Hofmann and coworkers.[57] It is reported by Feng and coworkers that, PVOH-coated PLGA nanoparticles exhibited a better stability, but a faster uptake to intestinal cells (2.9-folds) over the former PS nanoparticles of the same particle size, indicating that the PVOH surface also contributes to an efficient oral delivery of cancer drugs to the intestinal microenvironments.[66] In the case of current

gold@PVOH-*b*-PNVCL system, presence of PVOH segments also increases the hydrophilicity and colloidal stability of the nanpparticles, especially under physiological temperature (37 °C), in light of aggregation detected in gold@PNVCL aqueous suspension (S#3, LCST of 34 °C). Deeper insight into the role of PVOH on the interaction between gold@PVOH-*b*-PNVCL and biological systems could be an interesting topic of our following research. Moreover, compared with the conventional PEG, PVOH macromolecular chains also bear some remarkable advantages, like the presence of hydroxyl side groups as chemically-active sites (*e.g.* facile fluorescence or targeting moieties labelling), as well as specific affinity to some molecules, *e.g.* boronate derivatives,[56, 67] *etc*. To confirm the advantage of these PVOH-coated gold nanoparticles as *in vivo* DDS, the *in vivo* anti-tumour activity of the anti-tumour drugs-loaded gold@PVOH-*b*-PNVCL NPs will be investigated in our next study.

Conclusions

Thermo-responsive gold@PVOH-*b*-PNVCL NPs were *in-situ* fabricated by reducing $HAuCl_4$ with $NaBH_4$ in the presence of PVOH-b-PNVCL copolymers. Thermo-induced phase transition, as well as good reversibility, of the gold@PVOH-*b*-PNVCL NPs was detected upon variation in temperature. The resulting gold@PVOH-*b*-PNVCL NPs exhibited good colloidal stability above the LCST thanks to the steric stabilization by PVOH segments. A faster release of Nadolol® was detected above the LCST, suggesting the applicability as DDS, probably for anti-tumour chemotherapeutics. Cytotoxicity assessment showed a good biocompatibility of the gold@PVOH-*b*-PNVCL NPs with the fibroblast L929 cell line. This kind of thermo-responsive gold@PVOH-*b*-PNVCL NPs exhibits the potential to be used as DDS and controlled drug release. More work could still be done to exploit some other aspects of this system before developing as an effective DDS, such as improved drug loading capacity, synergistic phototherapy and light-activated chemotherapy, as well as biomedical imaging of the gold modality, *etc*.

Acknowledgements

The authors thank the Belgian National Funds for Scientific Research (F.R.S.-FNRS), the European Community in the frame of Erasmus Mundus International doctoral school IDS-FunMat and the Science Policy Office of the Belgian Federal Government (PAI VII-05) for their financial support. The authors are also grateful to the GIGA-imaging and flow cytometry platform of the University of Liège for their help with CLSM and FACS measurements, and Dr Christine Labrugère (CECAMA, Univ. Bordeaux) for performing the XPS analysis. C.D. is Research Director and A.D. is Research Associate by the F.R.S.-FNRS.

Notes and references

[a] *Center for Education and Research on Macromolecules (CERM), University of Liege, B6 Sart Tilman, B-4000 Liège, Belgium. Fax: (32)4-36663497; Tel: (32)4-3663565;* c.jerome@ulg.ac.be, christophe.detrembleur@ulg.ac.be

[b] *Laboratory of Mammalian Cell Culture (GIGA-R), University of Liège, B6 Sart Tilman, B-4000 Liège, Belgium*

[c] *CNRS, Univ. Bordeaux, ICMCB, UPR 9048, F-33600 Pessac, France Fax: +33 540 002 761, Tel: +33 540 002 651,* duguet@icmcb.u-bordeaux1.fr

† Electronic Supplementary Information (ESI) available: calibration curve of Nadolol®, *in-situ* UV/*vis* spectra of the gold@PVOH-*b*-PNVCL NPs growth, DLS, XRD and XPS patterns of gold@PVOH-*b*-PNVCL NPs, UV/*vis* spectra of gold NPs suspension during gradual heating, cumulative release profiles of Nadolol®-loaded gold@PVOH-*b*-PNVCL NPs suspension under alternating 37/40°C treatment, dependence of uptake amount of gold@PVOH-*b*-PNVCL NPs within MEL-5 cell line on incubation period and concentration, *etc*. See DOI: 10.1039/b000000x/

1. O. Veiseh, J. W. Gunn and M. Q. Zhang, *Adv. Drug. Delive. Rev.*, 2010, **62**, 284-304.
2. K. C. Petkar, S. S. Chavhan, S. Agatonovik-Kustrin and K. K. Sawant, *Crit. Rev. Ther. Drug*, 2011, **28**, 101-164.
3. D. Schmaljohann, *Adv. Drug. Delive. Rev.*, 2006, **58**, 1655-1670.
4. S. Cajot, N. Lautram, C. Passirani and C. Jerome, *J. Control. Release*, 2011, **152**, 30-36.
5. J. Liu, C. Detrembleur, M. Hurtgen, A. Debuigne, M.-C. De Pauw-Gillet, S. Mornet, E. Duguet and C. Jérôme, *Polym. Chem.*, 2014, **5**, 77-88.
6. M. Marguet, C. Bonduelle and S. Lecommandoux, *Chem. Soc. Rev.*, 2013, **42**, 512-529.
7. C. Legros, M.-C. De Pauw-Gillet, K. C. Tam, S. Lecommmandoux and D. Taton, *Polym. Chem.*, 2013, **4**, 4801-4808.
8. J. Song, J. Zhou and H. Duan, *J. Am. Chem. Soc.*, 2012, **134**, 13458-13469.
9. A. Al Zaki, D. Joh, Z. Cheng, A. L. B. De Barros, G. Kao, J. Dorsey and A. Tsourkas, *ACS Nano*, 2013.
10. S. Pearson, W. Scarano and M. H. Stenzel, *Chem. Commun.*, 2012, **48**, 4695-4697.
11. Y. Zhong, C. Wang, L. Cheng, F. Meng, Z. Zhong and Z. Liu, *Biomacromolecules*, 2013, **14**, 2411-2419.
12. E. Locatelli, W. Bost, M. Fournelle, J. Llop, L. Gil, F. Arena, V. Lorusso and M. C. Franchini, *J. Nanopart. Res.*, 2014, **16**, 1-9.
13. A. Topete, M. Alatorre-Meda, P. Iglesias, E. M. Villar-Alvarez, S. Barbosa, J. A. Costoya, P. Taboada and V. Mosquera, *ACS Nano*, 2014.
14. J. You, Z. Wang, Y. Du, H. Yuan, P. Zhang, J. Zhou, F. Liu, C. Li and F. Hu, *Biomaterials*, 2013, **34**, 4510-4519.
15. F. Wang, Y. C. Wang, S. Dou, M. H. Xiong, T. M. Sun and J. Wang, *Acs Nano*, 2011, **5**, 3679-3692.
16. Y. Lee, S. H. Lee, J. S. Kim, A. Maruyama, X. Chen and T. G. Park, *J. Control. Release*, 2011, **155**, 3-10.
17. Y. Tao, J. Han, C. Ye, T. Thomas and H. Dou, *J. Mater. Chem.*, 2012, **22**, 18864-18871.
18. M. W. Ambrogio, C. R. Thomas, Y. L. Zhao, J. I. Zink and J. F. Stoddart, *Acc. Chem. Res.*, 2011, **44**, 903-913.
19. M. Treguer-Delapierre, J. Majimel, S. Mornet, E. Duguet and S. Ravaine, *Gold Bull.*, 2008, **41**, 195-207.
20. E. A. Boisselier, D. Astruc, *Chem. Soc. Rev.* 2009, **38**. 1759-1782.
21. J. Zhang, M. Zhang, K. Tang, F. Verpoort and T. Sun, *Small*, 2014, **10**, 32-46.
22. A. Aqil, H. J. Qiu, J. F. Greisch, R. Jerome, E. De Pauw and C. Jerome, *Polymer*, 2008, **49**, 1145-1153.
23. M. Beija, J. D. Marty and M. Destarac, *Chem. Commun.*, 2011, **47**, 2826-2828.
24. R. Contreras-Caceres, A. Sanchez-Iglesias, M. Karg, I. Pastoriza-Santos, J. Perez-Juste, J. Pacifico, T. Hellweg, A. Fernandez-Barbero and L. M. Liz-Marzan, *Adv. Mater.*, 2008, **20**, 1666-1670.
25. X. Y. Liu, F. Cheng, Y. Liu, H. J. Liu and Y. Chen, *J. Mater. Chem.*, 2010, **20**, 360-368.
26. J. D. Marty, S. Sistach, M. Beija, V. Rahal, A. Brulet, M. Destarac and C. Mingotaud, *Chem. Mater.*, 2010, **22**, 3712-3724.
27. C. A. Fustin, C. Colard, M. Filali, P. Guillet, A. S. Duwez, M. A. Meier, U. S. Schubert and J. F. Gohy, *Langmuir*, 2006, **22**, 6690-6695.
28. J. Liu, C. Detrembleur, M.C. De Pauw-Gillet, S. Mornet, E. Duguet and C. Jérôme, *Polym. Chem.*, 2014, **5**, 799-813.
29. K. Kusolkamabot, P. Sae-ung, N. Niamnont, K. Wongravee, M. Sukwattanasinitt and V. P. Hoven, *Langmuir*, 2013, **29**, 12317-12327.
30. S. Haga, O. Watanabe, T. Shimuzu, H. Imamura, K. Kobayashi, J. Kinoshta, H. Nagumo and T. Kajiwara, *Breast Cancer*, 1996, **3**, 33-37.

31. C. J. Orendorff, L. Gearheart, N. R. Jana and C. J. Murphy, *Phys. Chem. Chem. Phys.*, 2006, **8**, 165-170.
32. Y. Bao, W. An, C. H. Turner and K. M. Krishnan, *Langmuir*, 2010, **26**, 478-483.
33. M. Hurtgen, J. Liu, A. Debuigne, C. Jerome and C. Detrembleur, *J. Polym. Sci. Polym. Chem.*, 2012, **50**, 400-408.
34. A. Debuigne, R. Poli, C. Jerome, R. Jerome and C. Detrembleur, *Prog. Polym. Sci.*, 2009, **34**, 211-239.
35. M. Hurtgen, C. Detrembleur, C. Jerome and A. Debuigne, *Polym. Rev.*, 2011, **51**, 26.
36. I. Goldenberg, J. Bradley, A. Moss, S. McNitt, S. Polonsky, J. L. Robinson, M. Andrews and W. Zareba, *J. Cardiovasc. Elect.*, 2010, **21**, 893-901.
37. A. Debuigne, J. R. Caille and R. Jerome, *Macromolecules*, 2005, **38**, 5452-5458.
38. L. Jiang, J. Guan, L. L. Zhao, J. Li and W. S. Yang, *Colloid. Surface A*, 2009, **346**, 216-220.
39. C. C. Chen, Y. P. Lin, C. W. Wang, H. C. Tzeng, C. H. Wu, Y. C. Chen, C. P. Chen, L. C. Chen and Y. C. Wu, *J. Am. Chem. Soc.*, 2006, **128**, 3709-3715.
40. A. H. Pakiari and Z. Jamshidi, *J Phys Chem A*, 2007, **111**, 4391-4396.
41. J. M. Kinyanjui, D. W. Hatchett, J. A. Smith and M. Josowicz, *Chem. Mater.*, 2004, **16**, 3390-3398.
42. G. H. Jiang, L. Wang and W. X. Chen, *Mater. Lett.*, 2007, **61**, 278-283.
43. S. J. Lee, G. Park, D. Seo, D. Ka, S. Y. Kim, I. S. Chung and H. Song, *Chem. Eur. J.*, 2011, **17**, 8466-8471.
44. Y. Gao, P. Jiang, D. Liu, H. Yuan, X. Yan, Z. Zhou, J. Wang, L. Song, L. Liu and W. Zhou, *J. Phys. Chem. B*, 2004, **108**, 12877-12881.
45. L. Qiu, F. Liu, L. Zhao, W. Yang and J. Yao, *Langmuir*, 2006, **22**, 4480-4482.
46. M. Q. Zhu, L. Q. Wang, G. J. Exarhos and A. D. Q. Li, *J. Am. Chem. Soc.*, 2004, **126**, 2656-2657.
47. Y. Shen, M. Kuang, Z. Shen, J. Nieberle, H. W. Duan and H. Frey, *Angew. Chem. Int. Ed.*, 2008, **47**, 2227-2230.
48. J. Qin, Y. S. Jo and M. Muhammed, *Angew. Chem. Int. Ed.*, 2009, **48**, 7845-7849.
49. M. Karg, I. Pastoriza-Santos, J. Perez-Juste, T. Hellweg and L. M. Liz-Marzan, *Small*, 2007, **3**, 1222-1229.
50. M. Karg, Y. Lu, E. Carbo-Argibay, I. Pastoriza-Santos, J. Perez-Juste, L. M. Liz-Marzan and T. Hellweg, *Langmuir*, 2009, **25**, 3163-3167.
51. J. Liu and Y. Lu, *Nat. Protoc.*, 2006, **1**, 246-252.
52. M. K. Corbierre, N. S. Cameron, M. Sutton, S. G. J. Mochrie, L. B. Lurio, A. Ruhm and R. B. Lennox, *J. Am. Chem. Soc.*, 2001, **123**, 10411-10412.
53. N. Nath and A. Chilkoti, *J. Am. Chem. Soc.*, 2001, **123**, 8197-8202.
54. S. Purushotham and R. V. Ramanujan, *Acta Biomater.*, 2010, **6**, 502-510.
55. Z. Zhu and S. A. Sukhishvili, *ACS Nano*, 2009, **3**, 3595-3605.
56. J. Liu, C. Detrembleur, A. Debuigne, M. C. De Pauw-Gillet, S. Mornet, L. Vander Elst, S. Laurent, E. Duguet and C. Jérôme, *J. Mater. Chem. B*, 2014. **2**, 1009-1023.
57. A. Petri-Fink, B. Steitz, A. Finka, J. Salaklang and H. Hofmann, *Eur. J. Pharm. Biopharm.*, 2008, **68**, 129-137.
58. J. Liu, C. Detrembleur, A. Debuigne, M.-C. De Pauw-Gillet, S. Mornet, L. Vander Elst, S. Laurent, C. Labrugère, E. Duguet and C. Jérôme, *Nanoscale*, 2013, **5**, 11464-11477.
59. J. Liu, C. Detrembleur, S. Mornet, E. Duguet and C. Jerome, *J. Control. Release*, 2013, **172**, e39.
60. M. Mahmoudi, A. Simchi and M. Imani, *J. Phys. Chem. C*, 2009, **113**, 9573-9580.
61. A. Petri-Fink, M. Chastellain, L. Juillerat-Jeanneret, A. Ferrari and H. Hofmann, *Biomaterials*, 2005, **26**, 2685-2694.
62. G. Storm, S. O. Belliot, T. Daemen and D. D. Lasic, *Adv. Drug. Delive. Rev.*, 1995, **17**, 31-48.
63. H. Otsuka, Y. Nagasaki and K. Kataoka, *Adv. Drug. Delive. Rev.*, 2003, **55**, 403-419.
64. A. S. Karakoti, S. Das, S. Thevuthasan and S. Seal, *Angew. Chem. Int. Ed.*, 2011, **50**, 1980-1994.
65. T. Shehata, K. I. Ogawara, K. Higaki and T. Kimura, *Int. J. Pharm.*, 2008, **359**, 272-279.
66. K. Yin Win and S. S. Feng, *Biomaterials*, 2005, **26**, 2713-2722.
67. D. Roy, J. N. Cambre and B. S. Sumerlin, *Prog. Polym. Sci.*, 2010, **35**, 278-301.

Graphical abstract

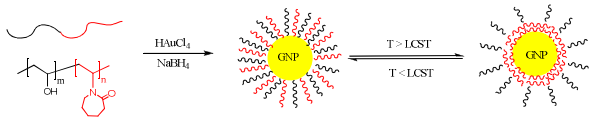

Preparation of thermo-responsive poly(vinyl alcohol)-*b*-poly(*N*-vinylcaprolactam) copolymer-stabilized gold nanoparticles for drug delivery